Rayleigh-Taylor instability in binary condensates

S. Gautam and D. Angom
Physical Research Laboratory, Navarangpura, Ahmedabad 380 009, India
(Received 9 September 2009; revised manuscript received 3 October 2009; published 17 May 2010)

We propose a well-controlled experimental scheme to initiate and examine the Rayleigh-Taylor instability in two-species Bose-Einstein condensates. We identify the ^{85}Rb-^{87}Rb mixture as an excellent candidate to observe experimentally. The instability is initiated by tuning the ^{85}Rb-^{85}Rb interaction through a magnetic Feshbach resonance. We show that the observable signature of the instability is the damping of the radial oscillations. We also propose a semianalytic scheme to determine the stationary state of binary condensates with the Thomas-Fermi approximation for axisymmetric traps.

DOI: 10.1103/PhysRevA.81.053616 PACS number(s): 03.75.Mn, 03.75.Kk

I. INTRODUCTION

Rayleigh-Taylor instability (RTI) sets in when a lighter fluid supports a heavier one in a gravitational field or when a lighter fluid pushes a heavier one. It leads to turbulent mixing of the two fluids as the perturbations at the interface grow exponentially. It is present across a wide spectrum of phenomena in nature. The turbulent mixing in astrophysics, inertial confinement fusion, and geophysics originates from RTI. In superfluids RTI sets up crystallization waves at the superfluid-solid interface. This has been observed in ^{4}He [1]. Despite the ubiquitous nature and importance of the RTI, controlled experiments are difficult and rare. However, we show that two-species Bose-Einstein condensates (TBECs) or binary condensates in a trap are ideal systems for a controlled study of RTI in superfluids. In a recent work [2], the magnetic-field-gradient-induced RTI at the interface of TBEC, which consists of two hyperfine states of ^{87}Rb, was analyzed. In the present work we propose a different mechanism to set up the RTI in TBECs and study the impact on the collective excitations. The remarkable feature of TBECs, absent in the single-component BECs, is the phenomenon of phase separation. The TBECs, which are realized in a mixture of two hyperfine states of ^{87}Rb [3], are rich systems for exploring nonlinear phenomena. Numerous theoretical works have examined different aspects of TBECs. These include stationary states [4–7], modulational instability [8–10], collective excitations [11–14], and domain-wall solitons [15]. Another instability related to the RTI, which has attracted growing interest, is the Kelvin-Helmholtz instability (KHI). The prerequisites of the KHI are phase separation and relative tangential velocities at the interface. Quantum KHIs have been observed in experiments with ^{3}He [16] and recently studied theoretically for TBECs [17].

To initiate the RTI we consider a TBEC confined in a harmonic trapping potential, where all the interatomic interactions are repulsive. We choose the ground state in the immiscible domain as the initial state. It is a phase-separated configuration where the species with the stronger intraspecies repulsive interaction surrounds the other [18,19]. Here the trapping potential is an analog of the gravitational potential, and we may consider the species with the stronger intraspecies repulsive interaction as the lighter fluid. We then increase the intraspecies repulsive interaction of the inner species by increasing the scattering length through a Feshbach resonance. A critical state is reached when the repulsive interactions of the inner and outer species are equal. The system is unstable to any further increase because the intraspecies repulsive interaction of the inner species is higher. This is the quantum analog of the RTI in fluid dynamics. As a case study, we choose the TBEC of a ^{85}Rb-^{87}Rb mixture. In this system, the ^{85}Rb intraspecies interaction is tunable through a Feshbach resonance [20] and was recently used to study the miscibility [21] of the TBEC. More recently, the dynamical pattern formation during the growth of this system was theoretically investigated [10]. The other feature is that the interspecies ^{85}Rb-^{87}Rb interaction is also tunable and well studied [22]. Considering the parameters of the experimental realization, we choose the axisymmetric (cigar-shaped) trap geometry.

II. PHASE-SEPARATED CIGAR-SHAPED TBECS

In the mean-field approximation, the TBEC is described by a set of coupled Gross-Pitaevskii (GP) equations

$$\left(\frac{-\hbar^2}{2m_i}\nabla^2 + V_i(\rho,z) + \sum_{j=1}^{2} U_{ij}|\psi_j|^2\right)\psi_i(\rho,z) = \mu_i\psi_i(\rho,z), \tag{1}$$

where $i = 1,2$ is the species index. Here $U_{ii} = 4\pi\hbar^2 a_{ii}/m_i$, where m_i is the mass and a_{ii} is the s-wave scattering length, is the intraspecies interaction, and $U_{ij} = 2\pi\hbar^2 a_{ij}/m_{ij}$, where $m_{ij} = m_i m_j/(m_i + m_j)$ is the reduced mass, with a_{ij} as the interspecies scattering length, is the interspecies interaction, and μ_i is the chemical potential of the ith species. To study the RTI, we consider the phase-separated state ($U_{12} > \sqrt{U_{11}U_{22}}$) in the axisymmetric trapping potentials with coincident centers,

$$V_i(\rho,z) = \frac{m_i\omega^2}{2}\left(\alpha_i^2\rho^2 + \lambda_i^2 z^2\right), \tag{2}$$

where ω is the smaller of the two radial trapping frequencies, and α_i and λ_i are the scaling factors of the radial and axial trapping frequencies, respectively. In the present work, we choose $\alpha_i > \lambda_i$ to generate cigar-shaped potentials, and U_{ij}'s are all positive. By neglecting the interspecies overlap,

the Thomas-Fermi (TF) solutions of the densities $n_i(\rho,z) = |\psi_i(\rho,z)|^2$ are

$$|\psi_i(\rho,z)|^2 = \frac{[\mu_i - V_i(\rho,z)]}{U_{ii}}. \quad (3)$$

The chemical potentials μ_i are fixed through the normalization conditions. When $\alpha_i \gg \lambda_i$, the interface of the phase-separated state is planar and the species having a larger scattering length sandwiches the other one [18]. This is clearly visible in the first column of Fig. 3, which shows the typical ground-state density profile of the cigar-shaped TBEC.

For further analysis, let $z = \pm L_1$ be the planes separating the two components and $\pm L_2$ be the spatial extent of the outer species along the z axis. The density distributions n_1 and n_2 of the TBEC are

$$n_1(\rho,z) = \frac{\mu_1 - V_1(\rho,z)}{U_{11}}, \quad -L_1 < z < L_1, \quad (4)$$

$$n_2(\rho,z) = \frac{\mu_2 - V_2(\rho,z)}{U_{22}}, \quad L_1 < |z| < L_2. \quad (5)$$

This assumes no spatial overlap between the two species. The problem of determining the stationary state is then equivalent to calculating L_1. Theoretically, L_1 can be determined by minimizing the total energy of the TBEC with a fixed number of particles of each species. If N_i and ρ_i are the number of atoms and the radial size of the ith species, respectively, then

$$N_i = 2\pi \int_0^{\rho_i} \rho\, d\rho \int_{-L_i}^{L_i} dz |\psi_i(\rho,z)|^2. \quad (6)$$

From the TF approximation

$$N_1 = 2\pi \left(\frac{\omega^2 L_1^5 m_1 \lambda_1^4}{20 U_{11} \alpha_1^2} - \frac{L_1^3 \lambda_1^2 \mu_1}{3 U_{11} \alpha_1^2} + \frac{L_1 \mu_1^2}{\omega^2 m_1 U_{11} \alpha_1^2} \right), \quad (7)$$

$$N_2 = 4\pi \left[\frac{4\sqrt{2}\mu_2^2 \sqrt{\frac{\mu_2}{\omega^2 \lambda_2^2 m_2}}}{15\omega^2 m_2 U_{22} \alpha_2^2} + \frac{L_1}{120 U_{22} \alpha_2^2} \left(5\omega^2 L_1^4 m_2 \lambda_2^4 - \frac{8\omega^2 m_2 \left(L_1^2 \lambda_2^2\right)^{5/2}}{\lambda_2 L_1} + 20 L_1^2 \lambda_2^2 \mu_2 - \frac{60\mu_2^2}{\omega^2 m_2} \right) \right]. \quad (8)$$

The total energy of the binary condensate is

$$E = \int dV \left[V_1(\rho,z)|\psi_1(\rho,z)|^2 + V_2(\rho,z)|\psi_2(\rho,z)|^2 + \frac{1}{2} U_{11} |\psi_1(\rho,z)|^4 + \frac{1}{2} U_{22} |\psi_2(\rho,z)|^4 \right]. \quad (9)$$

We minimize E numerically with Eqs. (7) and (8) as constraints to obtain the required value of L_1. By substituting the value of L_1 back into Eqs. (7) and (8), we can determine μ_1 and μ_2. Thus Eqs. (7)–(9) uniquely define the stationary state of the TBEC.

As mentioned earlier, we consider the parameters of the recent experiment [21] with ^{85}Rb and ^{87}Rb as the first and second species, respectively, in the case study. In the experiment the radial trapping frequencies are identical ($\alpha_i = 1$), and the scale factors or the anisotropy parameters of the axial trapping frequencies λ_1 and λ_2 are 0.022 and 0.020, respectively. The scattering lengths are $a_{11} = 51a_0$, $a_{22} = 99a_0$, and $a_{12} = a_{21} = 214a_0$, and we take $N_i = 50\,000$. For this set of parameter values the plot in Fig. 1 shows the variation of E as a function of L_1. The value of L_1 where the minimum of E occurs is $32.3a_{\rm osc}$. Here the unit of length $a_{\rm osc} = \sqrt{\hbar/m_1\omega}$ with the radial trapping frequency $\omega = 130$ Hz. This is in agreement with the numerical result $33.8a_{\rm osc}$ calculated using the split-step Crank-Nicholson method with imaginary-time propagation [23]. We refer to this state as phase I, where ^{85}Rb and ^{87}Rb are at the center and flanks, respectively.

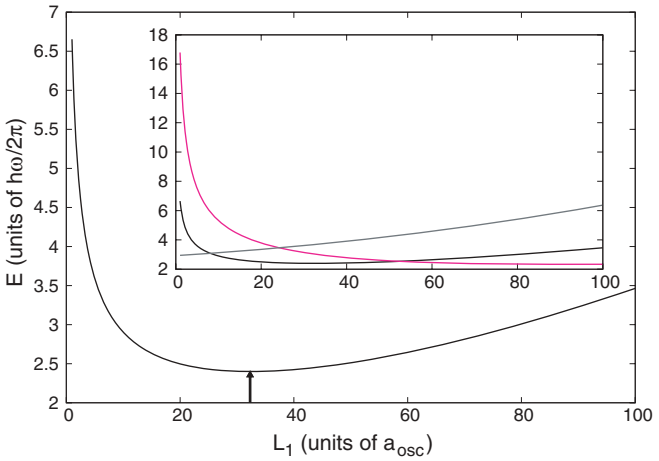

FIG. 1. (Color online) The variation in energy E with L_1 in a phase-separated regime. The upward arrow indicates the position of minimum E at $L_1 = 32.3a_{\rm osc}$. The inset shows the same plot along with the variation of μ_1 and μ_2 with respect to L_1, and the magenta (light gray) and gray curves correspond to μ_1 and μ_2, respectively.

We have also calculated the expressions for obtaining the ground state for trapping potentials whose centers do not coincide,

$$V_1(\rho,z) = \frac{m_1\omega^2}{2}\left(\alpha_1^2\rho^2 + \lambda_1^2 z^2\right), \quad (10)$$

$$V_2(\rho,z) = \frac{m_2\omega^2}{2}\left[\alpha_2^2\rho^2 + \lambda_2^2 (z - z_0)^2\right], \quad (11)$$

where z_0 is the separation of the two trap centers along the z axis. The expressions are much more complicated; however, the numerical and semianalytic results are in agreement.

III. BINARY CONDENSATE EVOLUTION

In the fluid dynamics parlance, the gradient of the trapping potentials is the equivalent of gravity and the dynamics of the condensates is modeled as potential flows. The dynamical evolution of the interface is then described through a combination of the continuity equation, Euler's equation, and Bernoulli's theorem with suitable boundary conditions [24,25]. For a phase-separated TBEC with a planar interface along the xy plane, a linear stability analysis shows that a small perturbation at the interface has independent modes of the form $A(s)e^{i(k_x x + k_y y) + st}$. Here k_x and k_y are wave numbers along x and y coordinates, s is the temporal decay constant, and

$A(s)$ is the amplitude of the mode. After solving the linearized equations [24,25], we get

$$s = \pm \left(\frac{\sqrt{k_x^2 + k_y^2} m\omega^2 \lambda^2 L_1 (n_2 - n_1)}{n_1 + n_2} \right)^{1/2}. \quad (12)$$

The densities of the condensates n_1 and n_2 are at a point (ρ, L_1) on the interface. We recollect that the n_1 and n_2 refer to the densities of the species at the center and flanks, respectively. To simplify the analysis, we consider $m_1 = m_2 = m$ and $\lambda_1 = \lambda_2 = \lambda$ while deriving relation (12).

The decay constant s is imaginary and the interface is stable when $n_1 > n_2$ but it oscillates when perturbed. However, when $n_1 < n_2$ the value of s is real and any perturbation, however small, grows exponentially. This is the prerequisite for RTI in binary condensates. From the TF approximation, this condition is equivalent to $a_{11} > a_{22}(\mu_1 - V)/(\mu_2 - V)$. Here V is the trapping potential of the two species at the interface. In normal fluids with RTI, the lighter fluid rises to the top as bubbles and the heavier fluid sinks as fingerlike extensions until the entire bulk of the lighter fluid is on top of the denser one. On the other hand, binary condensates in a similar situation evolve in a very different way.

To examine the dynamical evolution of the binary condensate with RTI, we choose phase I ($a_{11} < a_{22}$) as the initial state. In this phase, the ^{87}Rb BEC at the flanks is considered as resting over the ^{85}Rb BEC at the center. To set up a RTI, we increase a_{11} until $a_{11} > a_{22}(\mu_1 - V)/(\mu_2 - V)$ through the ^{85}Rb-^{85}Rb magnetic Feshbach resonance [20]. However, we maintain $U_{12} > \sqrt{U_{11}U_{22}}$ so that the TBEC remains in the immiscible domain. This is an unstable state, and we refer to this as phase Ia. The stationary state of the TBEC that corresponds to the new parameters is phase separated and similar in structure to the initial state but with the species interchanged. Let us call the stationary state that corresponds to the new parameters phase II. The binary condensate should dynamically evolve from phase Ia to phase II. However, unlike in normal fluids with RTI, there are no bulk flows of either ^{85}Rb or ^{87}Rb atoms across the interface. Instead the condensates expand with interference effects and modulations. At the same time, there is also tunneling. These events occur due to the coherence in the quantum liquids. To examine the evolution, we solve the pair of time-dependent GP equations

$$i\hbar \frac{\partial \psi_i(\rho,z)}{\partial t} = \left(\frac{-\hbar^2}{2m_i} \nabla^2 + V_i(\rho,z) + \sum_{j=1}^{2} U_{ij} |\psi_j|^2 \right) \psi_i(\rho,z), \quad (13)$$

which describe the dynamical evolution of the TBEC. During evolution the density profiles are approximated as

$$n_i(\rho,z) = n_i^{\mathrm{eq}}(\rho,z) + \delta n_i(\rho,z). \quad (14)$$

Here $n_i^{\mathrm{eq}}(\rho,z)$ and $\delta n_i(\rho,z)$ are the equilibrium density and density fluctuations arising from the increase in a_{11}, respectively. From the hydrodynamic approximations, $\delta n_i(\rho,z)$ or the collective modes follow the equations

$$m_i \frac{\partial^2}{\partial t^2} \delta n_i = \nabla n_i \cdot \nabla \sum_{j=1}^{2} U_{ij} \delta n_j + n_i \nabla^2 \sum_{j=1}^{2} U_{ij} \delta n_i. \quad (15)$$

Consider $\delta n_i(\rho,z,t) = b_i(t)\rho^l \exp(\pm il\phi)$ as the form of the solution. Here $b_i(t)$ subsumes the time-dependent part of the solution arising from the temporal variation of the amplitude and l is an integer. Then as $\nabla^2 \delta n_i = 0$, only the first term on the right-hand side remains in the equation. The profile of the interface acquires a complex pattern as it evolves under the influence of the RTI. This increases the area of the interface and couples the two species more strongly through the interspecies interaction. Furthermore, as the inner species expands and penetrates in the outer species, the density decreases and hence the mean-field energy decreases. This damps the radial oscillations of the inner component. In the miscible phase, the evolution equation simplifies to

$$\ddot{b}_i = -\frac{l\omega^2}{U_{ii}} (U_{ii} b_i + U_{ij} b_j). \quad (16)$$

We can also get a similar set of coupled equations for the other form of the collective modes $\delta n_i(\rho,z,t) = b_i(t) z \rho^{l-1} \exp[\pm i(l-1)\phi]$. In this case, the prefactor is $(l - 1 + \lambda_i^2)$ instead of l. In either of the cases, the equations are similar to two coupled oscillators. For the phase-separated state, the form of the TF solutions is significantly different from the miscible solution. We resort to numerical schemes to solve the coupled-GP equations with RTI. An analytical description is difficult because the interface geometry evolves to a highly complex structure.

IV. NUMERICAL RESULTS

A. TBEC evolution with RTI

As mentioned earlier, to examine the evolution of TBEC with RTI, we choose the phase-I state as the initial state. We then change a_{11} to $80a_0$, $102a_0$, $200a_0$, $306a_0$, $408a_0$, and $780a_0$; the last value is in the miscible parameter region. The dynamical variables, which are the coarse-grained representatives of the evolution, are ρ_{rms} and z_{rms}, the rms radial and axial sizes, respectively.

When a_{11} is increased to $80a_0$, the ^{85}Rb condensate oscillates radially to accommodate excess repulsion energy. This is the only available degree of freedom as tight confinement along the z axis, arising from ^{87}Rb at the flanks, restricts axial oscillations. In the TF approximation, the effective potential is $V_{\mathrm{eff}} = V + (\mu_2 - V)U_{12}/U_{22}$. The angular frequency of the oscillation is $\approx 0.32\omega$. This is close to one of the eigenmodes of the Bogoliubov equations. The temporal variation of ρ_{rms} is shown as the plots in the inset in Fig. 2. These show that the oscillations of the ^{87}Rb are sympathetically initiated and arise from the coupling between the two condensate species. The oscillations are more prominent with a smaller number of atoms.

There is a change in the nature of oscillations when the new value of a_{11} is such that $a_{11} > a_{22}(\mu_1 - V)(\mu_2 - V)$. The corresponding stationary state has ^{87}Rb and ^{85}Rb at the core and flanks, respectively. The ρ_{rms} oscillation frequency is the same as in the $a_{11} < a_{22}$ case, but there is a temporal decay of the amplitude until it equilibrates. This is due to the expansion of ^{85}Rb along the z axis and is an unambiguous signature of the RTI. The expansion is clearly discernible in the density profile of the condensates shown in Fig. 3. The main plot

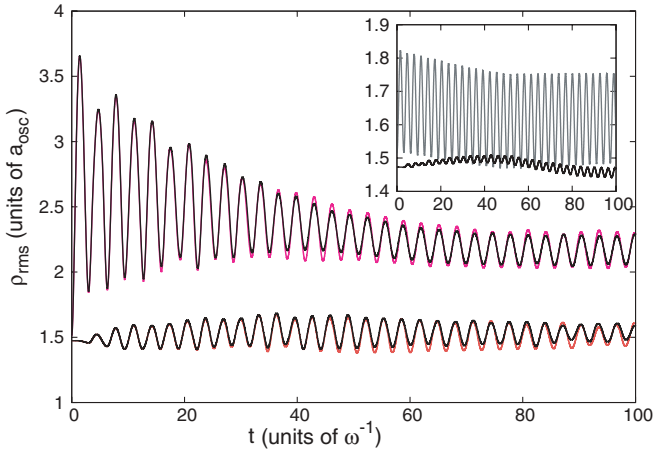

FIG. 2. (Color online) The temporal variation of $\rho_{\rm rms}$ for ^{85}Rb and ^{87}Rb when a_{11} is changed from $51a_0$ to $408a_0$. In the main plot, the upper and lower black curves correspond to the evolution of ^{85}Rb and ^{87}Rb, respectively. The magenta (light gray) and red (gray) curves correspond to evolution with loss terms. The plot in the inset shows the variation in $\rho_{\rm rms}$ of ^{85}Rb (gray) and ^{87}Rb (black) without loss terms.

in Fig. 2 shows a temporal variation of $\rho_{\rm rms}$ for $a_{11} = 408a_0$ close to the miscible domain. There is a strong correlation between the decay rate and the nature of oscillations. For a_{11} marginally larger than a_{22}, the ^{85}Rb condensate tunnels through the ^{87}Rb condensate, whereas at larger values the ^{85}Rb condensate expands and spreads into the ^{87}Rb condensate.

A dramatic change in the nature of the coupled oscillations occurs when $U_{12} < \sqrt{U_{11}U_{22}}$, that is, when the TBEC is in the miscible domain. The ^{85}Rb condensate expands through the ^{87}Rb cloud, and the two species undergo radial oscillations which have a beat pattern. Figure 4 shows the $\rho_{\rm rms}$ when a_{11} is increased to $780a_0$. Besides the radial oscillations, which are to be expected when $a_{11} > a_{22}(\mu_1 - V)/(\mu_2 - V)$, the axial size $z_{\rm rms}$ increases steadily. This accommodates the excess repulsion energy along the axial direction. Along with the oscillations, there are density fluctuations reminiscent of modulational instability. It must be mentioned that in earlier works [8,9] modulational instability in the miscibility domain was analyzed in depth. For the present case, the detailed analysis of modulational instability will be the subject of a future publication.

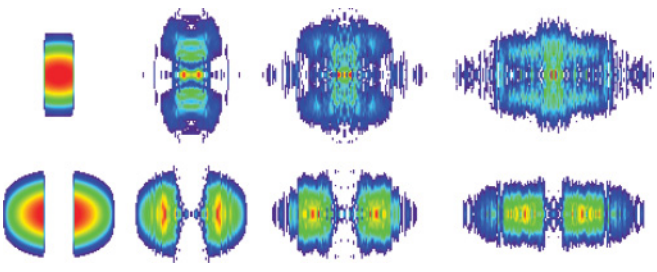

FIG. 3. (Color online) Evolution of the TBEC with RTI. The first and second rows are density profiles of ^{85}Rb and ^{87}Rb BECs, respectively, after increasing a_{11} to $408a_0$. Starting from the left, the density profiles are at 0, 24.5, 49.0, and 73.5 ms after the increase of a_{11}.

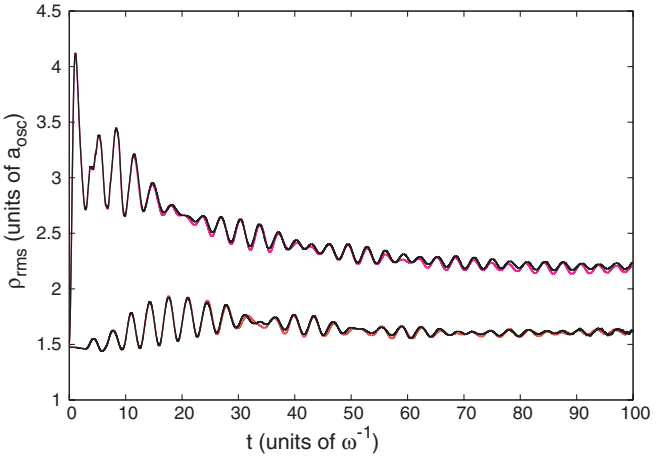

FIG. 4. (Color online) The variation in $\rho_{\rm rms}$ for ^{85}Rb and ^{87}Rb with time when a_{11} is increased from $51a_0$ to $780a_0$. In the main plot, the upper and lower black curves correspond to the evolution of ^{85}Rb and ^{87}Rb, respectively. The magenta (light gray) and red (gray) curves correspond to the evolution with the loss terms.

B. Evolution with loss terms

We also study the effect of loss terms, which arise from inelastic collisions, on the evolution of the condensate. There are two types of inelastic collisions that lead to the loss of atoms from the trap: dipolar relaxation where the two atoms change their spin states after binary collision and three-body recombination where three atoms collide, resulting in the formation of a diatomic molecule. To model the effect of loss of atoms from the trap, we add the phenomenological loss term

$$\frac{-i\hbar}{2}\left(\sum_{j=1}^{2} K_{2(ij)}|\psi_j(r,z)|^2 + K_{3i}|\psi_i(r,z)|^4\right) \qquad (17)$$

to the right-hand side of Eq. (13). Here $K_{2(ii)}$ and $K_{2(ij)}$ with $j \neq i$ are the two-body dipolar loss rate coefficients for collisions between same and different species, and K_{3i} are the three-body recombination loss rate coefficients.

In the experiment by Papp *et al.* [21], it is possible to vary a_{11} from $51a_0$ to $900a_0$ by tuning the magnetic field in the range 164.6–158.6 G [26]. In this range of the magnetic field, $K_{2(22)}$ and $K_{2(12)} = K_{2(21)}$ are approximately constant [27]. Based on a previous work [27], the inelastic two-body loss rate coefficients of the ^{85}Rb-^{87}Rb TBEC in a magnetic field of 161 G are $K_{2(11)} \simeq 10^{-14}$ cm^3 s^{-1}, $K_{2(22)} \simeq 4.5 \times 10^{-17}$ cm^3 s^{-1}, and $K_{2(12)} = K_{2(21)} \simeq 1.6 \times 10^{-16}$ cm^3 s^{-1}. For $K_{2(11)}$, the maximum value occurs when a_{11} is $51a_0$ and decreases at most by an order of magnitude for higher values of a_{11}.

For the inelastic three-body loss rate coefficients, the value of K_{31} is minimum when a_{11} is $51a_0$ [20] and changes by more than two orders of magnitude for higher values of a_{11}, but K_{32} remains constant. From previous works, rate coefficients for ^{85}Rb and ^{87}Rb are 1.7×10^{-27} cm^6 s^{-1} (near resonance) and 3.8×10^{-29} cm^6 s^{-1} [28], respectively. Between the two loss mechanisms, within a magnetic field range of 158–162 G the two-body losses of ^{85}Rb dominate over three-body losses [20]. Taking these factors into account, we consider the previously mentioned loss rates as the appropriate values when a_{11} is increased to $408a_0$ and $780a_0$ in our numerical simulations.

For the case of a_{11} increased to $80a_0$, we consider $K_{2(11)} \simeq 2.5 \times 10^{-14}$ cm^3 s^{-1} and $K_{31} = 3.8 \times 10^{-31}$ cm^6 s^{-1} while the other loss rate coefficients remain unchanged. We find that when the RTI sets in, the nature of oscillations of $\rho_{\rm rms}$ do not change significantly with the inclusion of the loss term. The maximum change is $\approx$4% and this is evident from Figs. 2 and 4. This implies that the decay of the $\rho_{\rm rms}$ oscillation amplitude can be mainly ascribed to the RTI and not to the loss of atoms from the trap.

V. CONCLUSIONS

We have examined the onset of the Rayleigh-Taylor instability in TBEC and identified the observable signature in the dynamics. We have specifically chosen the experimentally well-studied ^{85}Rb-^{87}Rb mixture as a case study and propose observing RTI with the ^{85}Rb-^{85}Rb Feshbach resonance. By starting from $a_{11} < a_{22}$, the RTI sets in when the TBEC is tuned to $a_{11} > a_{22}(\mu_1 - V)/(\mu_2 - V)$ in the TF approximation. The damping of $\rho_{\rm rms}$ oscillations of ^{85}Rb, the species at the core, marks the onset of RTI. To analyze the stationary state, we have proposed a semianalytic scheme, applicable when $\lambda \ll 1$, to minimize the energy functional with the TF approximation. The results are in excellent agreement with the numerical results. In the parameter regime $\lambda \ll 1$ the interface is also planar and the RTI is more prominent.

ACKNOWLEDGMENTS

We thank S. A. Silotri, B. K. Mani, and S. Chattopadhyay for very useful discussions. We acknowledge the help of P. Muruganandam while doing the numerical calculations.

[1] S. N. Burmistrov, L. B. Dubovskii, and V. L. Tsymbalenko, Phys. Rev. E **79**, 051606 (2009).
[2] K. Sasaki, N. Suzuki, D. Akamatsu, and H. Saito, Phys. Rev. A **80**, 063611 (2009).
[3] C. J. Myatt, E. A. Burt, R. W. Ghrist, E. A. Cornell, and C. E. Wieman, Phys. Rev. Lett. **78**, 586 (1997).
[4] T.-L. Ho and V. B. Shenoy, Phys. Rev. Lett. **77**, 3276 (1996).
[5] H. Pu and N. P. Bigelow, Phys. Rev. Lett. **80**, 1130 (1998).
[6] M. Trippenbach, K. Goral, K. Rzazewski, B. Malomed, and Y. B. Band, J. Phys. B **33**, 4017 (2000).
[7] P. Ao and S. T. Chui, Phys. Rev. A **58**, 4836 (1998).
[8] K. Kasamatsu and M. Tsubota, Phys. Rev. Lett. **93**, 100402 (2004).
[9] T. S. Raju, P. K. Panigrahi, and K. Porsezian, Phys. Rev. A **71**, 035601 (2005).
[10] S. Ronen, J. L. Bohn, L. E. Halmo, and M. Edwards, Phys. Rev. A **78**, 053613 (2008).
[11] R. Graham and D. Walls, Phys. Rev. A **57**, 484 (1998).
[12] H. Pu and N. P. Bigelow, Phys. Rev. Lett. **80**, 1134 (1998).
[13] D. Gordon and C. M. Savage, Phys. Rev. A **58**, 1440 (1998).
[14] A. A. Svidzinsky and S. T. Chui, Phys. Rev. A **68**, 013612 (2003).
[15] S. Coen and M. Haelterman, Phys. Rev. Lett. **87**, 140401 (2001).
[16] R. Blaauwgeers, V. B. Eltsov, G. Eska, A. P. Finne, R. P. Haley, M. Krusius, J. J. Ruohio, L. Skrbek, and G. E. Volovik, Phys. Rev. Lett. **89**, 155301 (2002).
[17] H. Takeuchi, N. Suzuki, K. Kasamatsu, H. Saito, and M. Tsubota, Phys. Rev. B **81**, 094517 (2010).
[18] This is a symmetry-preserving configuration. The other configuration, the symmetry-breaking solution, is energetically not favorable.
[19] K. Kasamatsu, Y. Yasui, and M. Tsubota, Phys. Rev. A **64**, 053605 (2001).
[20] J. L. Roberts, N. R. Claussen, S. L. Cornish, and C. E. Wieman, Phys. Rev. Lett. **85**, 728 (2000).
[21] S. B. Papp, J. M. Pino, and C. E. Wieman, Phys. Rev. Lett. **101**, 040402 (2008).
[22] S. B. Papp and C. E. Wieman, Phys. Rev. Lett. **97**, 180404 (2006).
[23] P. Muruganandam and S. K. Adhikari, Comput. Phys. Commun. **180**, 1888 (2009).
[24] P. Drazin and W. Reid, *Hydrodynamic Stability* (Cambridge University Press, New York, 2004).
[25] S. Chandrasekhar, *Hydrodynamic and Hydromagnetic Stability* (Dover, New York, 1981).
[26] S. L. Cornish, N. R. Claussen, J. L. Roberts, E. A. Cornell, and C. E. Wieman, Phys. Rev. Lett. **85**, 1795 (2000).
[27] J. P. Burke Jr., J. L. Bohn, B. D. Esry, and C. H. Greene, Phys. Rev. Lett. **80**, 2097 (1998).
[28] B. D. Esry, C. H. Greene, and J. P. Burke, Phys. Rev. Lett. **83**, 1751 (1999).